


## First-principles calculations of physical properties and superconductivity of orthorhombic ScRuSi and ZrRhSi

H. Y. Uzunok,<sup>1,2</sup> S. Bağcı,<sup>1</sup> Ertuğrul Karaca,<sup>2</sup> H. M. Tütüncü<sup>1,2</sup> ,<sup>1,2</sup> and G. P. Srivastava<sup>3</sup>

<sup>1</sup>Sakarya Üniversitesi, Fen-Edebiyat Fakültesi, Fizik Bölümü, 54187 Adapazarı, Turkey

<sup>2</sup>Sakarya Üniversitesi, BIMAYAM Biyomedikal, Manyetik ve Yarıiletken Malzemeler Araştırma Merkezi, 54187 Adapazarı, Turkey

<sup>3</sup>School of Physics, University of Exeter, Stocker Road, Exeter EX4 4QL, United Kingdom



(Received 1 June 2020; revised 14 August 2020; accepted 9 October 2020; published 22 October 2020)

We have performed *ab initio* pseudopotential calculations of the structural, electronic, elastic, mechanical, vibrational, electron-phonon interaction, and superconducting properties of ScRuSi and ZrRhSi. An assessment of their elastic and mechanical properties reveals that ScRuSi is a ductile compound, while ZrRhSi is a brittle compound. For both compounds electronic energy bands in the vicinity of the Fermi level originate from the *d* states of transition-metal atoms. The Eliashberg spectral function reveals that low-frequency phonon modes due to coupled motions of transition-metal atoms are more involved in the process of scattering of electrons than the high-frequency modes due to the vibrations of Si atoms. The average electron-phonon coupling parameter is calculated to be 0.54 for ScRuSi and 0.84 for ZrRhSi from the integration of the Eliashberg spectral function. It is found that the relatively weaker electron-phonon interaction in ScRuSi makes its superconducting transition temperature value ( $T_c = 3.23$  K) considerably lower than that of ZrRhSi ( $T_c = 10.45$  K).

DOI: [10.1103/PhysRevB.102.134508](https://doi.org/10.1103/PhysRevB.102.134508)

### I. INTRODUCTION

Ternary equiatomic intermetallic  $TT'X$  ( $T, T' =$  transition metals;  $X =$  boron, carbon, or nitrogen) compounds have been providing interesting research topics because of their outstanding structural [1–10] and magnetic [11–21] properties. These intermetallic compounds usually exist in two structure forms with equal atomic compositions. They occur either in the orthorhombic (o) TiNiSi-type structure with space group Pnma [1] or the hexagonal (h) ZrNiAl-type structure with space group  $P\bar{6}m2$  [2]. Both phases of  $TT'X$  compounds are layer structures. Furthermore, both phases exhibit superconductivity and hence major attention was paid towards their superconducting properties [22–31]. Usually, the superconducting transition temperatures of hexagonal materials are considerably higher than those of orthorhombic materials. For example, the superconducting transition temperature ( $T_c$ ) of h-ZrRuP, h-HfRuP, h-ZrRuSi, and h-ZrRuAs is about 12 K [22–25,28–30] while the  $T_c$  values of o-ZrRuP, o-ZrRuSi, o-ZrIrSi, o-HfIrSi, o-YIrSi, o-NbRhP, and o-TaRhP lies between 2 and 5 K [25,27,30]. Therefore, the ZrNiAl-type structure appears to be suitable for the enhancement of superconducting temperature. However, it is worth noting that the compound ZrRhSi with the TiNiSi-type structure is the particular case with its  $T_c$  value of above 10 K [32]. In addition to this, investigation of low-temperature electrical and magnetic properties of MoRuP [33] with the orthorhombic TiNiSi-type structure reveals that this compound becomes a superconductor at 15.5 K, which is the highest  $T_c$  value among all the ternary equiatomic intermetallic  $TT'X$  compounds. Heat capacity and electrical resistivity measurements [34] indicate that o-YRhAl exhibits superconductivity with a  $T_c$

value of 0.9 K. Furthermore, o-MgPtSi has been discovered to display superconductivity with a  $T_c$  value of 2.5 K [35].

In recent years, research has concentrated on the discovery of Sc-including  $TT'X$ -type superconductors because Sc is close to Zr and Hf with respect to atomic radius and constitutes many similar structures [36,37]. Additionally, Sc shows a superconducting transition above  $\sim 60$  GPa, which reaches 20 K at 107 GPa [38,39]. In 2016, Okamoto and co-workers reported that h-ScIrP becomes a superconductor at 3.4 K by using electrical resistivity, magnetization, and heat capacity measurements of polycrystalline samples prepared by a solid-state reaction method [40]. On the basis of heat capacity data in a zero magnetic field, this compound is proposed to be a weakly coupled Bardeen-Cooper-Schrieffer superconductor [40]. Moreover, their electronic structure calculations [40] reveal that the electronic states of ScIrP near the Fermi level are dominated by the Sc *3d* and Ir *5d* states. In the same year, powder x-ray diffraction experiments [41] showed that ScRhP crystallizes in the hexagonal ZrNiAl-type structure. Furthermore, resistivity, magnetization, and heat capacity data [41] reveal that h-ScRhP shows superconductivity with a  $T_c$  value of 2 K which is lower than that of its *5d* analog h-ScIrP [40]. In 2017, the physical property measurements of o-ScRuSi indicated that this material becomes a superconductor at 3.1 K [42].

On the theoretical side, there has been a great deal of interest in the study of structural and electronic properties of ternary equiatomic intermetallic  $TT'X$  compounds due to their superconducting properties. The extended Huckel tight-binding model [43] is used to investigate the electronic properties of h-ZrRuP and o-ZrRuP. The value of the density of states at the Fermi level [ $N(E_F)$ ] is reported to be

0.21 and 0.29 states/eV atom for h-ZrRuP and o-ZrRuP, respectively [43]. Although the  $T_c$  value of o-ZrRuP is four times smaller than that of h-ZrRuP, its  $N(E_F)$  value is larger than that of h-ZrRuP. This result signals that the high  $T_c$  difference between them cannot be explained in terms of their  $N(E_F)$  values. The electronic structure calculation has been realized on h-ZrRuX ( $X = \text{P, As, Si}$ ) by using the full-potential linearized augmented plane-wave method within the local-density approximation [44]. This calculation reveals that electronic states near the Fermi level for all these superconductors are dominated by the  $d$  states of Ru atoms [44]. The electronic properties of h-MoRuP, o-MoRuP, h-ZrRuP, and o-ZrRuP have been investigated by using the method of orthogonalized linear combinations of atomic orbitals [45]. A critical assessment of their electronic structures [45] suggests that h-MoRuP might possess a  $T_c$  in excess of 20 K. In 2015, *ab initio* pseudopotential calculations were performed for the structural, elastic, and mechanical properties of the ternary silicides ScT<sub>2</sub>Si ( $T = \text{Co, Ni, Cu, Ru, Rh, Pd, Ir, Pt}$ ) by Sebehi and co-workers [46]. According to this theoretical study [46], the ScT<sub>2</sub>Si ( $T = \text{Ru, Pd, Pt}$ ) compounds behave in a ductile manner, while the ScT<sub>2</sub>Si ( $T = \text{Co, Ni, Cu, Rh, Ir}$ ) compounds behave in a brittle manner.

Although several calculations [43–45] have been made on the structural, elastic, and electronic properties of ternary equiatomic intermetallic  $TT'X$  compounds, theoretical studies on their lattice dynamics and electron-phonon interaction were totally overlooked in the literature until 2016. In 2016, Tütüncü and co-workers [47] researched electron-phonon interaction in o-MgPtSi. This theoretical study [47] reveals that MgPtSi is a conventional phonon-mediated compound with a medium electron-phonon coupling strength of 0.707. In the same year, the electron-phonon interaction properties of h-ScIrP were analyzed by using the first-principles calculation method [48]. This theoretical work [48] reveals that the spin-orbit coupling makes a considerable impact on the electron-phonon interaction of this superconductor due to a large nuclear charge of the Ir atom since the strength of this effect depends proportionally on the square of the atomic number  $Z^4$ . Very recently, Bağcı and co-workers [49] have studied electron-phonon interaction in both phases of ZrRuP in order to explain why the  $T_c$  value of o-ZrRuP is considerably smaller than that of h-ZrRuP. This *ab initio* study [49] indicates that the lattice of o-ZrRuP is harder than that of h-ZrRuP which makes its electron-phonon coupling parameter (0.57) much smaller than the corresponding value of 1.25 for h-ZrRuP. Consequently, the  $T_c$  value of o-ZrRuP becomes much smaller than that of h-ZrRuP.

The motivation for this work is to discern the electronic and phonon structures, and relative strength of the electron-phonon coupling in contributing to bulk superconductivity in a newly discovered superconductor o-ScRuSi via comparison with its isostructural compound of o-ZrRhSi through *ab initio* pseudopotential calculations. In addition, strain-stress calculations [50] have been executed in order to obtain elastic properties of investigated superconductors. The average electron-phonon coupling parameter and logarithmic average of phonon frequency have been presented from the calculation of Eliashberg spectral functions. Using these quantities and the Migdal-Eliashberg approach [51,52], the

$T_c$  values of ScRuSi and ZrRhSi are computed and compared with experimentally reported values.

## II. METHOD

Our *ab initio* calculations have been performed in the framework of density functional theory by using the QUANTUM ESPRESSO simulation package [53,54]. The generalized gradient approximation (GGA) in the Perdew-Burke-Ernzerhof scheme [55] is used to obtain the exchange and correlation potential. The ion-electron interaction is modeled by using norm-conserving pseudopotentials [56] while a plane-wave cutoff energy of 60 Ry is utilized to specify the number of plane waves in expansion. The valance configuration of atoms has been considered as Zr( $5s^24d^2$ ), Sc( $4s^23d^1$ ), Rh( $5s^24d^7$ ), Ru( $5s^24d^6$ ), and Si( $3s^23p^2$ ). During the structural optimization, the crystal structure has been totally relaxed by the help of the Broyden-Fletcher-Goldfrab-Shanno minimization method [57], in which total energy has been minimized by changing the lattice parameters and atomic positions. Self-consistent solutions of the Kohn-Sham equations [58] have been approached by using a set of Monkhorst-Pack special  $\mathbf{k}$  points [59]. Integration over the Brillouin zone for structural properties has been executed by using special  $\mathbf{k}$  points produced with  $(6 \times 6 \times 6)$  Monkhorst-Pack mesh while a denser  $(24 \times 24 \times 24)$ - $\mathbf{k}$  mesh is used for the calculation of electronic properties.

Vibrational properties of both superconductors have been investigated within the framework of self-consistent density functional perturbation theory [53,54]. For the phononic calculations, integration over the Brillouin zone was executed by using a special set of 64 special  $\mathbf{k}$  points. As phononic calculations are computationally much more demanding than electronic calculations, we first calculated eight dynamical matrices on the  $2 \times 2 \times 2$  Monkhorst-Pack grid. Then, they were Fourier-transformed into real space and thus the force constants were determined, which were used to establish phonon frequencies for any  $\mathbf{q}$  points.

The combination of the Migdal-Eliashberg theory [51,52] and the linear response theory [53,54] has been used for the calculation of electron-phonon interaction in the studied compounds. Within the Migdal-Eliashberg approach [51,52], the Eliashberg spectral function, expressed in terms of phonon linewidth  $\gamma_{\mathbf{q}j}$ , has the following form:

$$\gamma_{\mathbf{q}j} = 2\pi\omega_{\mathbf{q}j} \sum_{\mathbf{k}nm} |g_{(\mathbf{k}+\mathbf{q})m;\mathbf{k}n}^{\mathbf{q}j}|^2 \delta(\varepsilon_{\mathbf{k}n} - \varepsilon_F) \delta(\varepsilon_{(\mathbf{k}+\mathbf{q})m} - \varepsilon_F), \quad (1)$$

where the electron-phonon matrix element  $g_{(\mathbf{k}+\mathbf{q})m;\mathbf{k}n}^{\mathbf{q}j}$  is obtained self-consistently by the linear response theory [53,54]. Then, the Eliashberg spectral function [ $\alpha^2F(\omega)$ ] has the following form:

$$\alpha^2F(\omega) = \frac{1}{2\pi N(E_F)} \sum_{\mathbf{q}j} \frac{\gamma_{\mathbf{q}j}}{\hbar\omega_{\mathbf{q}j}} \delta(\omega - \omega_{\mathbf{q}j}), \quad (2)$$

where  $N(E_F)$  refers to the electronic density of states per atom and spin at the Fermi level. The electron-phonon coupling

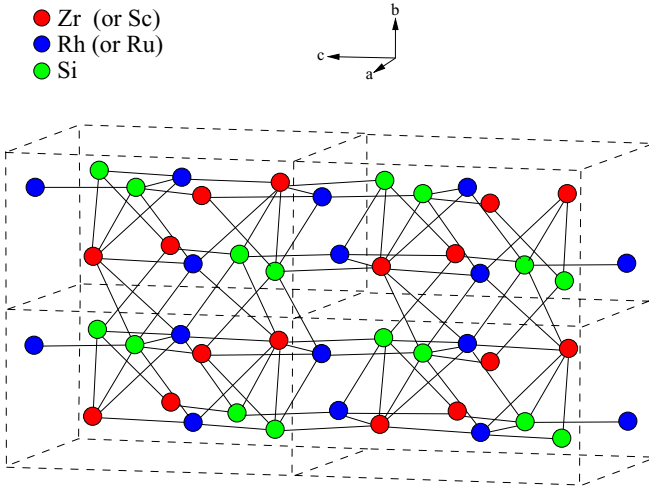


FIG. 1. The layer crystal structure of ZrRhSi (or ScRuSi) with an orthorhombic TiNiSi-type form. This structure includes layers which are filled with Zr (or Sc), Rh (or Ru), and Si atoms.

constant is given by the following form:

$$\lambda_{\mathbf{q}j} = \frac{\gamma_{\mathbf{q}j}}{\pi \hbar N(\epsilon_F) \omega_{\mathbf{q}j}^2}. \quad (3)$$

The integration of the Eliashberg spectral function gives the values of average electron-phonon coupling constant  $\lambda$  and logarithmically averaged frequency  $\omega_{\ln}$ :

$$\lambda = \int_0^\infty \frac{\alpha^2 F(\omega)}{\omega} d\omega, \quad (4)$$

$$\omega_{\ln} = \exp\left(2\lambda^{-1} \int_0^\infty \frac{d\omega}{\omega} \alpha^2 F(\omega) \ln \omega\right). \quad (5)$$

Finally, the superconducting critical temperature can be estimated using the Allen-Dynes modified McMillan formula [60–62]:

$$T_c = \frac{\omega_{\ln}}{1.2} \exp\left(-\frac{1.04(1 + \lambda)}{\lambda - \mu^*(1 + 0.62\lambda)}\right). \quad (6)$$

The above equation is reported to be highly accurate for superconductors when the value of the average electron-phonon coupling parameter is less than 1.5 [60–62]; it has successfully characterized the superconducting properties for many compounds indeed. In the above equation,  $\mu^*$  refers to the screening Coulomb pseudopotential, usually taking a typical

value between 0.10 and 0.13 [61,62]. In our calculations, its value is set to 0.11.

### III. RESULTS

#### A. Structural and electronic properties

Both intermetallic superconductors are reported to crystallize in the orthorhombic TiNiSi-type crystal structure which is displayed in Fig. 1. As can be appreciated from this figure, the orthorhombic phase of both compounds is constituted by layers which are filled with  $T$  (Zr or Sc),  $T'$  (Rh and Ru), and Si. The primitive unit cell of orthorhombic TiNiSi-type crystal structure contains 12 atoms with Wyckoff positions of 4(c)  $(x_T, 1/4, z_T)$  for four  $T$  (Sc or Zr) atoms, 4(c)  $(x_{T'}, 1/4, z_{T'})$  for four  $T'$  (Ru or Rh) atoms, and 4(c)  $(x_{Si}, 1/4, z_{Si})$  for Si atoms. Consequently, the orthorhombic TiNiSi-type crystal structure of both studied compounds is shaped by three lattice parameters ( $a$ ,  $b$ , and  $c$ ) and six inner coordinates ( $x_T$ ,  $x_{T'}$ ,  $x_{Si}$ ,  $z_T$ ,  $z_{T'}$ , and  $z_{Si}$ ). Full structural optimization is achieved by following the procedure described in our previous papers [63]. The determined values of lattice parameters, inner coordinates, bulk modulus, and its pressure derivative for ScRuSi are presented in Table I together with those of ZrRhSi. For comparison, existing experimental [32,42] results and previous theoretical [46] results are also included in this table. The maximum variation of calculated lattice parameters from their corresponding experimental values [32,42] is less than 1.5% for both intermetallic superconductors while the calculated inner parameters of ScRuSi are comparable with their experimental [42] results and their previous GGA [46] results. Unfortunately, we could not reach any experimental results for the inner coordinates of ZrRhSi. Furthermore, no experimental or theoretical results are available for the values of  $B$  and  $B'$  of both intermetallic superconductors.

The energy band dispersion of ScRuSi is displayed in Fig. 2(a). It is a three-dimensional metal since at least one dispersive band crosses the Fermi level. Figure 2(b) presents the total, and  $s$ ,  $p$ , and  $d$  partial density of states (DOS) at the Sc, Ru, and Si atomic sites. The lowest four bands lying between  $-9.7$  and  $-7.7$  eV originate from the hybridization of Si  $3s$  states with Ru  $5p$ , Ru  $4d$ , Sc  $4p$ , and Sc  $3d$  states and are separated by a gap of 2.8 eV from the near-Fermi valence bands. In the energy window from  $-4.9$  to  $-2.8$  eV, the intensity patterns of the partial DOS of Ru  $4d$  and Si  $3p$  states are similar, indicating these states are strongly hybridized between each other over this energy range. This implies the existence of covalent bonding in ScRuSi. Ru  $4d$  states

TABLE I. The calculated values of lattice parameters, internal parameters, bulk modulus ( $B$ ), and its pressure derivative ( $B'$ ) for orthorhombic ScRuSi and ZrRhSi and their comparison with corresponding experimental data and corresponding previous theoretical results.

Compound	$a$ (Å)	$b$ (Å)	$c$ (Å)	$(x_T, x_{T'}, x_{Si})$	$(z_T, z_{T'}, z_{Si})$	$B$ (GPa)	$B'$
ScRuSi	6.7007	4.1241	7.1064	(0.00236, 0.15788, 0.29714)	(0.68455, 0.06209, 0.38694)	149.3	4.01
Experimental [36]	6.6192	4.0972	7.0491	(−0.00061, 0.15778, 0.29412)	(0.68610, 0.05978, 0.38662)		
Experimental [42]	6.6222	4.1001	7.0446	(−0.00121, 0.15925, 0.29148)	(0.68441, 0.05922, 0.39004)		
GGA [46]	6.650	4.160	6.980	(−0.00665, 0.15720, 0.29410)	(0.68660, 0.06130, 0.38840)		
ZrRhSi	6.5903	3.9466	7.4938	(0.01898, 0.14857, 0.27719)	(0.68273, 0.06495, 0.38285)	182.3	4.84
Experimental [32]	6.5491	3.9181	7.4592				

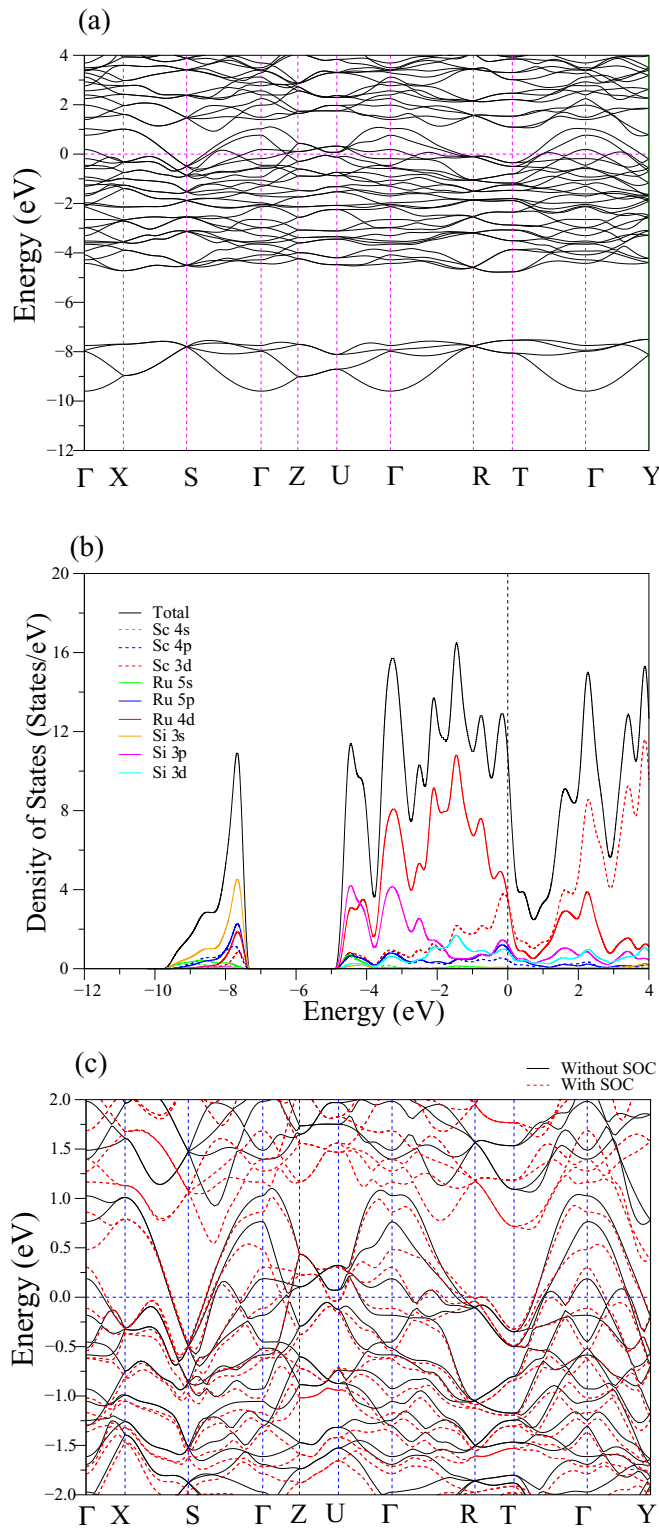


FIG. 2. (a) The calculated electronic band structure of ScRuSi along the most important axes of symmetry in the Brillouin zone of a simple orthorhombic lattice. The Fermi level is set to 0 eV. (b) Total and partial electronic density of states for ScRuSi. (c) The effect of spin-orbit coupling (SOC) on the near-Fermi electronic structure of ScRuSi.

constitute prominent DOS peaks between  $-2.8$  and  $-0.5$  eV. The electronic states in the vicinity of the Fermi level, which

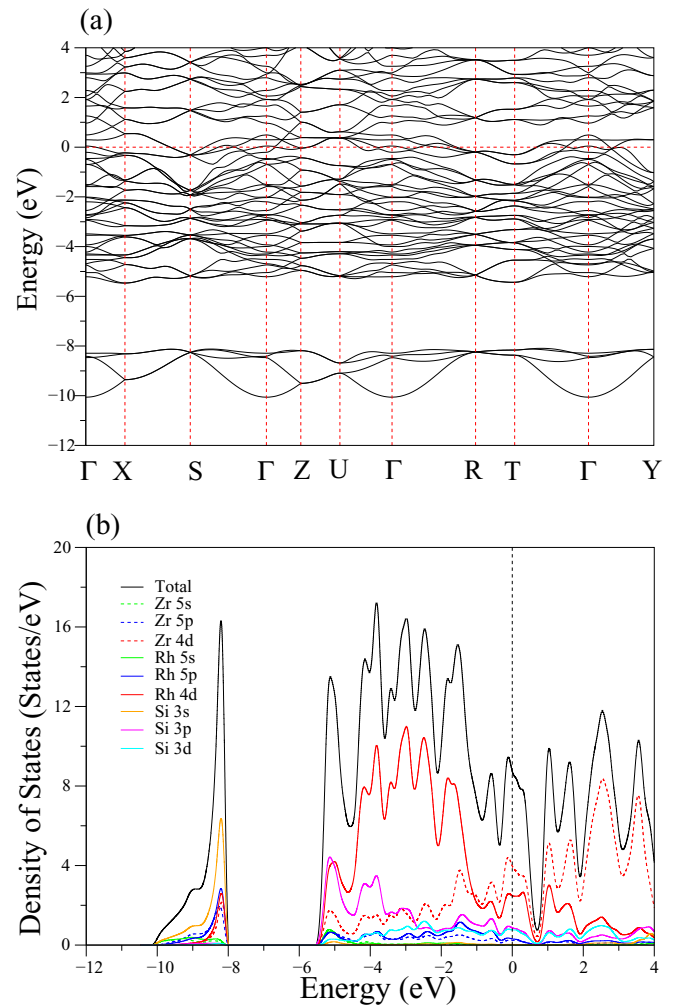


FIG. 3. (a) The calculated electronic band structure of ZrRhSi along the most important axes of symmetry in the Brillouin zone of a simple orthorhombic lattice. The Fermi level is set to 0 eV. (b) Total and partial electronic density of states for ZrRhSi.

mostly consist of Sc 3d and Ru 4d states, are important for superconductivity since Cooper pairs in the BCS theory are formed by electrons which have energies close to the Fermi level. The DOS at the Fermi level [ $N(E_F)$ ] for ScRuSi is estimated to be 9.848 states/eV, with Sc, Ru, and Si electronic states contributing 37%, 43%, and 20%, respectively. Distinctively, Sc 3d and Ru 4d states contribute almost equally to the value of  $N(E_F)$  within 32% and 33%, respectively. This confirms that Sc 3d and Ru 4d states may play a crucial role in the formation of the superconducting state for ScRuSi. Finally the effect of spin-orbit coupling (SOC) on the near-Fermi electronic bands of ScRuSi is shown in Fig. 2(c). This figure clearly shows that the energy changes of electronic bands due to SOC, however, remain small, in particular at the Fermi level. Also the  $N(E_F)$  value when the SOC is considered is calculated as 9.910 states/eV which differs 0.6% from the corresponding value calculated without SOC. Therefore, we do not consider this coupling in our further calculations.

The energy band dispersion of ZrRhSi is illustrated in Fig. 3(a). This material also shows a metallic character with

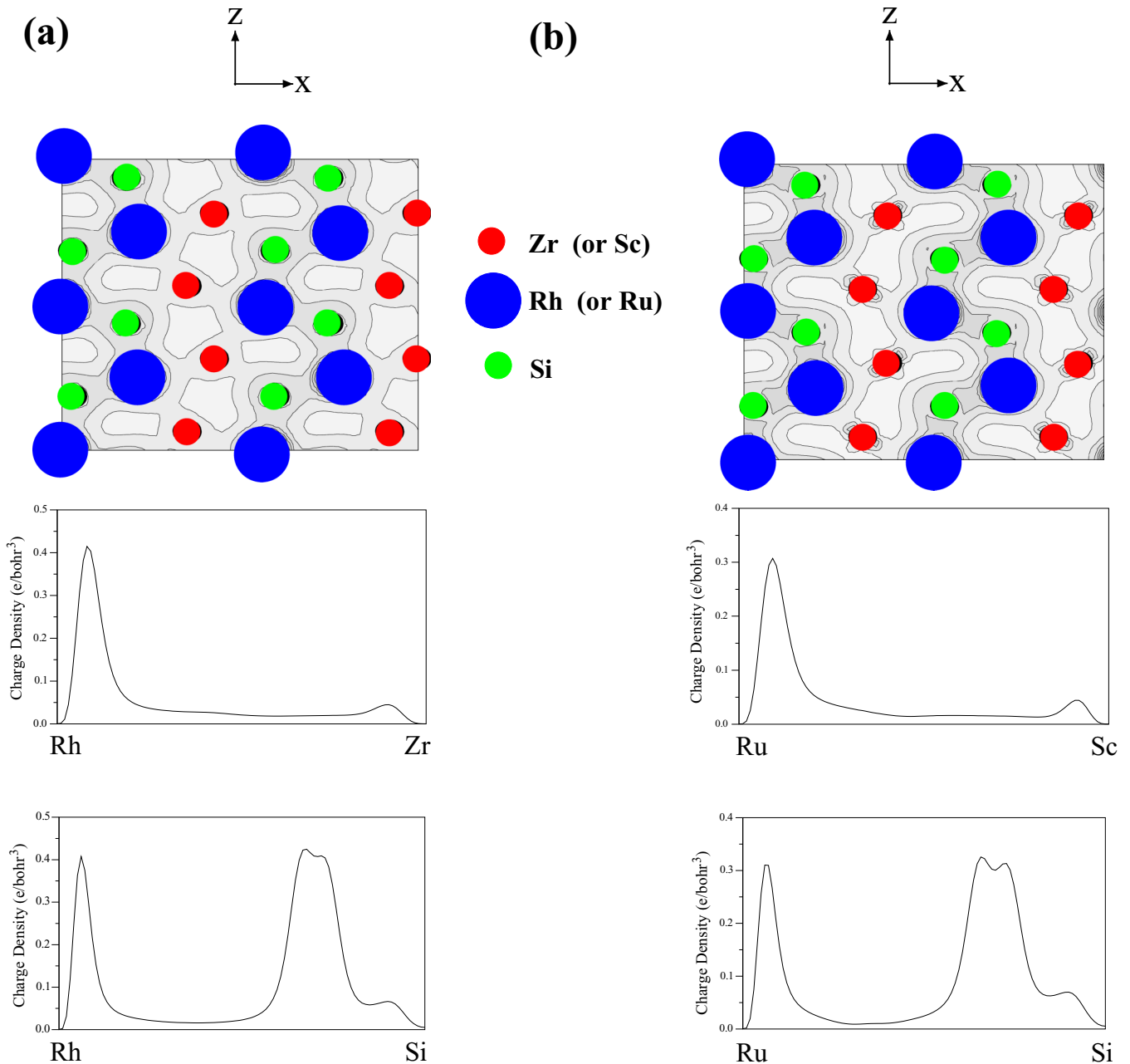


FIG. 4. Electronic charge density contour plot in the  $x$ - $z$  plane at  $y = 0$ , and comparison of the electronic charge density plots (a) along the Rh-Zr and Rh-Si bonds for ZrRhSi (the minimal and maximal values of the charge density are respectively 0.00024 and 0.43250) and (b) along the Ru-Sc and Ru-Si bonds for ScRuSi (the minimal and maximal values of the charge density are respectively 0.00048 and 0.32730).

at least one dispersive band crossing the Fermi level along all, except the R-T, considered symmetry directions. The total and partial DOS for ZrRhSi are displayed in Fig. 3(b). The valence DOS region splits into two obvious parts separated by a gap of 2.5 eV: the lower band extending from  $-10.1$  to  $-8.0$  eV and the upper part of chemical importance from  $-5.5$  eV up to the Fermi level. Therefore, the transition-metal bandwidth of ZrRhSi is 0.6 eV larger than that of ScRuSi. This result is expected because both transition metals of ZrRhSi have  $4d$  electrons rather than  $3d$  electrons. The lower part of the valence DOS region contains only one peak at  $-8.2$  eV, which is mainly composed of Si  $3s$  states with considerable contributions from the  $p$  and  $d$  states of both transition-metal

atoms. Several interesting peaks exist in the second part of the valence DOS region. In particular, the peak at  $-5.1$  eV mostly originates from significant hybridization between Rh  $4d$  and Si  $3p$  states, which signals a strong covalent interaction between these atoms. The features between  $-4.5$  and  $-0.8$  eV are contributed by Rh  $4d$  states with smaller contribution from the remaining electronic states.  $N(E_F)$  is 8.474 states/eV, with the percentage contributions from Zr, Rh, and Si atoms being roughly 49%, 33%, and 18%, respectively. The two largest contributions to the value of  $N(E_F)$  come from the  $4d$  states of Zr atoms (roughly 46%) and the  $4d$  states of Rh (roughly 29%). Therefore, in light of BCS theory, we can consider Zr  $d$  electrons as most efficient in the formation of a superconduct-

ing state for ZrRhSi. Although the  $T_c$  value of ZrRhSi (10.3 K) is considerably higher than that of ScRuSi (3.1 K), its  $N(E_F)$  value is smaller than that of ScRuSi. Eventually, the difference in their  $T_c$  values cannot be related to the difference in their  $N(E_F)$  values. Therefore, a sound explanation of this large  $T_c$  difference between the studied superconductors definitely needs phonon and electron-phonon interaction calculations on them. Although we do not show it in Fig. 3, the effect of SOC on the near-Fermi electronic bands of ZrRhSi is small.

To explain the bonding characteristics of ScRuSi and ZrRhSi, we have shown an electronic charge density contour plot in the  $x$ - $z$  plane at  $y = 0$ , and comparison of the electronic charge density plots along the Rh-Zr and Rh-Si bonds for ZrRhSi [Fig. 4(a)] and along the Ru-Sc and Ru-Si bonds for ScRuSi [Fig. 4(b)]. The plots in Figs. 4(a) and 4(b) confirm ionic bonding between Zr(Sc) and Rh(Ru) and covalent bonding between Rh(Ru) and Si atoms. These charge density plots provide a clear evidence of the ionic-covalent admixture bonding character within both studied compounds. Also, both materials' bonding shows similar characteristics which could be decided by the electronic charge density contour plot.

The Brillouin zone high-symmetry points and the calculated Fermi surface (FS) sheets of ZrRhSi and ScRuSi compounds are presented in Fig. 5, which are obtained by using the XCRYSDEN software [64]. The left and right columns correspond to the FS sheets for ZrRhSi and ScRuSi, respectively. In Fig. 5(b), one can see four FS sheets for the ZrRhSi compound. While the first two sheets show similar features with each other, the other two sheets are also similar to each other. The first FS forms nesting along the  $\Gamma$ -S direction while the second FS shows a more complex feature along  $\Gamma$ -X and  $\Gamma$ -Z directions. Both third and fourth FS sheets look like open-top hats and have nesting features along the  $\Gamma$ -R direction. On the other hand, the ScRuSi compound has five FS sheets and the first FS is barely formed by a tangential electronic band to the Fermi energy level. The second and third FS sheets have complex nesting properties that suggest that both of these have both hole and electron pocket features. Similar to ZrRhSi, the fourth and fifth sheets are similar to each other with some minor differences. These sheets look like waving sheets which have nesting features along the  $\Gamma$ -Z direction. We can deduce that the charge transport for both compounds is managed by both electrons and holes that could lead to a multiband superconductivity.

## B. Elastic and mechanical properties

We have employed the strain-stress approach [50] for the investigation of elastic properties for both studied superconductors. The symmetry of simple orthorhombic lattice produces nine independent elastic constants, viz.,  $C_{11}$ ,  $C_{12}$ ,  $C_{13}$ ,  $C_{22}$ ,  $C_{23}$ ,  $C_{33}$ ,  $C_{44}$ ,  $C_{55}$ , and  $C_{66}$ . Their calculated values for both superconductors are listed in Table II, together with previous GGA results [46] for ScRuSi. Generally, our results are in agreement with those in [46] except the value of  $C_{66}$  which we calculate to be more than two times larger. This large difference signals that experimental studies are certainly required for the elastic properties of ScRuSi.

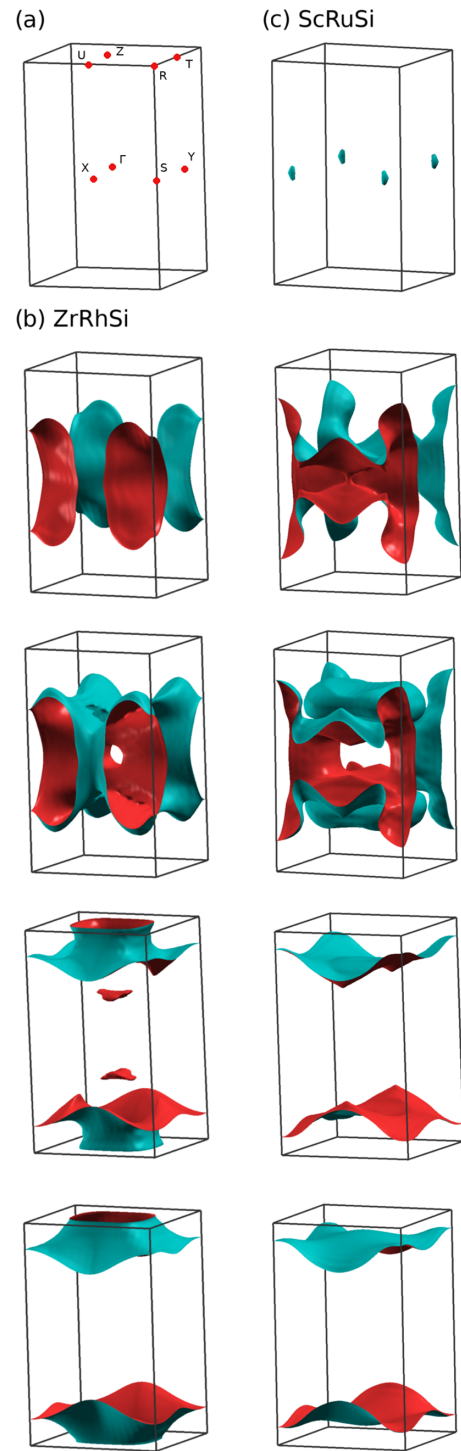


FIG. 5. (a) The high-symmetry points of simple orthorhombic structure, and the calculated three-dimensional Fermi surface sheets of (b) ZrRhSi and (c) ScRuSi compounds.

For an orthorhombic lattice, the mechanical stability criteria [65] are

$$C_{ii} > 0 \quad (i = 1, 6), \quad C_{11} + C_{22} - 2C_{12} > 0, \quad (7)$$

$$C_{22} + C_{33} - 2C_{23} > 0, \quad C_{11} + C_{33} - 2C_{13} > 0, \quad (8)$$

$$C_{11} + C_{22} + C_{33} + 2C_{12} + 2C_{13} + 2C_{23} > 0. \quad (9)$$

TABLE II. The estimated values of single crystal elastic constants and three Cauchy pressures ( $C_{12}$ - $C_{66}$ ,  $C_{13}$ - $C_{55}$ ,  $C_{23}$ - $C_{44}$ ) (in GPa) for orthorhombic superconductors ScRuSi and ZrRhSi.

Superconductor	$C_{11}$	$C_{12}$	$C_{13}$	$C_{22}$	$C_{23}$	$C_{33}$	$C_{44}$	$C_{55}$	$C_{66}$	$C_{12}$ - $C_{66}$	$C_{13}$ - $C_{55}$	$C_{23}$ - $C_{44}$
ScRuSi	233	91	96	226	151	223	73	61	85	6	35	71
GGA [46]	227	98	111	220	156	222	79	66	36	62	45	77
ZrRhSi	304	124	110	284	136	315	119	115	122	2	-5	17

Our calculated elastic constants for both superconductors satisfy the above stability criteria, indicating their mechanical stability in the orthorhombic TiNiSi-type crystal structure. As can be seen from Table II, there are three Cauchy pressures for the simple orthorhombic lattice:  $C_{12}$ - $C_{66}$ ,  $C_{13}$ - $C_{55}$ , and  $C_{23}$ - $C_{44}$  [66]. They can be used to define the bonding character of compounds. If their values are all positive, compounds are inclined to constitute bonds of metallic nature. Table II shows that the Cauchy pressures for ScRuSi are all positive, signaling stronger metallic bonding in it as compared to ZrRhSi.

The bulk modulus ( $B$ ), shear modulus ( $G$ ), Young's modulus ( $E$ ), and Poisson's ratio ( $\sigma$ ) can be derived by using the elastic constants and the Voigt-Reuss-Hill (VRH) approach [65,67–69]. Their calculated values for both superconductors are presented in Table III, together with previous GGA results for ScRuSi [46]. Our calculated value of  $B_H$  for ScRuSi is coherent with the GGA value in [46] since its value is independent from the value of  $C_{66}$ . However, our values of  $G_H$  and  $E$  for ScRuSi are larger than the values in [46] since they both depend on the value of  $C_{66}$ . Although we could not find any experimental results for the mechanical properties of both compounds, the  $B_H$  values compare very well with the values obtained from total energy calculations (see Table I). In addition to the three Cauchy pressures, the ratio of bulk to shear modulus ( $B_H/G_H$ ) [70] can be utilized to specify ductility or brittleness of a compound. If its value is greater than its limit value of 1.75, the compound has ductile character; otherwise it acts in a brittle manner. According to Table III, ScRuSi is a ductile superconductor while ZrRhSi is a brittle superconductor. Furthermore, the Poisson ratio [71] is also used to predict the brittleness and ductility. A Poisson ratio that is larger (smaller) than the limit value of 0.26 represents ductile (brittle) nature. The ductile character of ScRuSi is also confirmed by its Poisson ratio, while the corresponding value for ZrRhSi signals its brittle character. Even though both materials show similar bonding characteristics, the elastic nature could be related by the bonding strength which can be seen from the electronic charge density contour plot in Fig. 4.

Significant elastic anisotropy may give rise to microcracks in compounds [72]. Consequently, elastic anisotropy is a main

quantity to improve compound durability. Several anisotropic indexes can be utilized to define elastic anisotropy. In this work, the universal anisotropic index ( $A^U$ ) and the percent of anisotropy indexes ( $A_B$  and  $A_G$ ) are preferred. Their values can be derived from the following equations:

$$A^U = 5 \frac{G_V}{G_R} + \frac{B_V}{B_R} - 6 \geq 0, \quad (10)$$

$$A_B = \frac{B_V - B_R}{B_V + B_R}, \quad (11)$$

$$A_G = \frac{G_V - G_R}{G_V + G_R}. \quad (12)$$

Large deviation of these parameters from zero signals the anisotropic character of a compound. As shown in Table III, the  $A_B$  values of both superconductors are smaller than their  $A_G$  values, signaling that they are weakly anisotropic in bulk modulus. However, as can be seen from Table III, the difference between  $G_V$  and  $G_R$  values for both superconductors is larger than the corresponding difference between  $B_V$  and  $B_R$  values for them. Therefore, this difference considerably influences the value of  $A^U$ , which is a much better pointer for mechanical anisotropic properties. The bigger the value  $A^U$  is, the stronger the anisotropy of the compound is. Therefore, according to Table III, ScRuSi exhibits much stronger anisotropic character than ZrRhSi.

### C. Phonons and electron-phonon interaction

The zone center optical phonon modes of both superconductors can be classified by the irreducible representation of the point group  $D_{2h}$ . The group theory predicts the following symmetries of the zone center optical phonon modes:

$$\Gamma(D_{2h}) = 6A_g + 3B_{1g} + 6B_{2g} + 3B_{3g} \\ + 3A_u + 5B_{1u} + 2B_{2u} + 5B_{3u},$$

with all of them being singly degenerate. Using the polarization vectors, we define the symmetry of zone center optical phonon modes for both superconductors. Their calculated frequencies and electron-phonon coupling parameters

TABLE III. The estimated values of isotropic bulk modulus  $B_{VRH}$ , shear modulus  $G_{VRH}$ , Young's modulus  $E$  (all in GPa),  $B_H/G_H$  ratio, Poisson's ratio ( $\sigma$ ), the universal anisotropic index ( $A^U$ ), and percent anisotropy ( $A_B$ ,  $A_G$ ) for orthorhombic superconductors ScRuSi and ZrRhSi.

Superconductor	$B_V$	$B_R$	$B_H$	$G_V$	$G_R$	$G_H$	$E$	$B_H/G_H$	$\sigma$	$A^U$	$A_B$	$A_G$
ScRuSi	150.86	149.70	150.28	66.78	60.98	63.88	167.23	2.350	0.314	0.48330	0.00386	0.04539
GGA [46]			155			53	142	2.94	0.346			
ZrRhSi	182.69	182.53	182.61	106.77	103.82	105.29	264.96	1.734	0.258	0.14294	0.00044	0.01401

TABLE IV. Frequencies ( $\nu$  in THz), electron-phonon coupling parameters ( $\lambda$ ), and eigencharacters of zone center optical phonon modes for ScRuSi with the orthorhombic TiNiSi-type structure. The notations of I, R, and S refer to infrared active, Raman active, and silent modes, respectively. Dominant vibrated atoms in that frequencies are shown with bold text.

Mode	$\nu$	$\lambda$	Eigen characters	Mode	$\nu$	$\lambda$	Eigen characters
$A_u$ (S)	3.857	0.006	Sc+ <b>Ru</b> +Si	$B_{1u}$ (I)	3.876	0.021	Sc+ <b>Ru</b> +Si
$A_g$ (R)	3.944	0.022	Sc+ <b>Ru</b> +Si	$B_{1g}$ (R)	4.421	0.034	Sc+ <b>Ru</b> +Si
$B_{3u}$ (I)	4.433	0.009	<b>Sc</b> + Ru +Si	$B_{3g}$ (R)	4.434	0.012	Sc+ <b>Ru</b> +Si
$B_{2g}$ (R)	4.538	0.031	<b>Sc</b> + Ru +Si	$A_g$ (R)	4.957	0.021	<b>Ru</b> +Si
$A_g$ (R)	5.108	0.016	<b>Sc</b>	$B_{2g}$ (R)	5.314	0.031	Sc+ <b>Ru</b> +Si
$B_{3u}$ (I)	5.503	0.008	<b>Sc</b> +Ru+Si	$B_{1u}$ (I)	5.534	0.012	<b>Sc</b> +Ru+Si
$A_u$ (S)	5.621	0.006	<b>Sc</b>	$B_{1g}$ (R)	5.808	0.016	<b>Sc</b> +Ru+Si
$B_{2u}$ (I)	5.917	0.005	<b>Sc</b> +Ru	$B_{3u}$ (I)	5.978	0.009	<b>Sc</b> +Ru+Si
$B_{2g}$ (R)	5.989	0.032	<b>Sc</b> +Ru+Si	$A_g$ (R)	6.152	0.016	<b>Sc</b> +Ru+Si
$B_{1u}$ (I)	6.431	0.019	<b>Sc</b> +Ru	$B_{3g}$ (R)	6.539	0.009	<b>Sc</b>
$B_{2g}$ (R)	7.224	0.012	<b>Sc</b>	$B_{1u}$ (I)	8.665	0.009	Sc+ <b>Si</b>
$B_{3u}$ (I)	8.806	0.010	Sc+ <b>Si</b>	$A_g$ (R)	8.844	0.010	Sc+ <b>Si</b>
$B_{2g}$ (R)	9.104	0.018	Sc+ <b>Si</b>	$B_{3u}$ (I)	10.411	0.004	Sc+Ru+ <b>Si</b>
$B_{1u}$ (I)	10.416	0.006	Sc+Ru+ <b>Si</b>	$A_g$ (R)	10.537	0.004	Sc+Ru+ <b>Si</b>
$B_{2g}$ (R)	10.549	0.012	<b>Si</b>	$A_u$ (S)	10.567	0.001	<b>Si</b>
$B_{3g}$ (R)	10.612	0.009	Ru+ <b>Si</b>	$B_{2u}$ (I)	11.030	0.004	Sc+Ru+ <b>Si</b>
$B_{1g}$ (R)	11.057	0.003	Ru+ <b>Si</b>				

with defined symmetries and the dominant additives from the atomic species are presented in Tables IV and V for ScRuSi and ZrRhSi, respectively. As can be derived from these tables, the average value of zone center phonon frequencies ( $\bar{\nu}$ ) amounts to 7.036 THz for ScRuSi and 6.776 THz for ZrRhSi. These results reveal that the  $\bar{\nu}$  value of ZrRhSi is softer than the corresponding value of ScRuSi. On the other hand, the total value of the zone center electron-phonon coupling parameter  $\lambda$  for ZrRhSi equals 1.568, which is much larger than the corresponding value of 0.437 for ScRuSi. Consequently, our zone center phonon calculations reveal that electron-phonon interaction in ScRuSi is much weaker than that in ZrRhSi, which makes, using the Allen-Dynes modified McMillan

formula [see Eq. (6)], its  $T_c$  considerably lower than that of ZrRhSi.

The phonon band dispersion of ScRuSi is illustrated in Fig. 6(a). The phonon spectrum is divided into three apparent regions by two phonon band gaps of 1.2 and 1.0 THz: a low-frequency band (LFB) (0–7.2 THz), a mid-frequency band (MFB) (8.4–9.1 THz), and a high-frequency band (HFB) (10.1–11.4 THz). These bands contain 24, 4, and 8 phonon branches, respectively. Analyzing the partial phonon DOS in Fig. 6(b), one can observe that, as anticipated, Si as the lightest in this superconductor dominates at high frequencies. The MFB and HFB regions of the DOS are correlated almost completely to Si. However, a considerably smaller Si additive

TABLE V. Frequencies ( $\nu$  in THz), electron-phonon coupling parameters ( $\lambda$ ), and eigencharacters of zone center optical phonon modes for ZrRhSi with the orthorhombic TiNiSi-type structure. The notations of I, R, and S refer to infrared active, Raman active, and silent modes, respectively.

Mode	$\nu$	$\lambda$	Eigen characters	Mode	$\nu$	$\lambda$	Eigen characters
$B_{2g}$ (R)	3.599	0.292	Zr+ <b>Rh</b> +Si	$A_u$ (S)	3.713	0.008	Zr+ <b>Rh</b> +Si
$A_g$ (R)	3.785	0.317	Zr+ <b>Rh</b> +Si	$B_{1u}$ (I)	4.148	0.009	Zr+ <b>Rh</b> +Si
$B_{1g}$ (R)	4.287	0.059	<b>Zr</b> +Si	$B_{3u}$ (I)	4.306	0.071	<b>Zr</b> +Si
$A_g$ (R)	4.308	0.097	<b>Zr</b> +Rh+Si	$A_u$ (S)	4.654	0.005	<b>Zr</b> +Rh
$B_{3g}$ (R)	4.779	0.031	<b>Zr</b> +Rh+Si	$B_{3g}$ (R)	4.862	0.037	Zr+ <b>Rh</b> +Si
$B_{2g}$ (R)	4.994	0.033	<b>Zr</b> +Si	$B_{3u}$ (I)	5.079	0.018	<b>Zr</b> +Rh+Si
$B_{1g}$ (R)	5.114	0.032	Zr+ <b>Rh</b> +Si	$A_g$ (R)	5.173	0.072	Zr+ <b>Rh</b> +Si
$B_{2u}$ (I)	5.188	0.032	<b>Zr</b> +Rh	$B_g$ (R)	5.289	0.116	Zr+ <b>Rh</b> +Si
$B_{1u}$ (I)	5.546	0.020	Zr+ <b>Rh</b> +Si	$B_{3u}$ (I)	5.546	0.005	<b>Zr</b> +Rh+Si
$B_{2g}$ (R)	5.594	0.046	Zr+ <b>Rh</b> +Si	$B_{2g}$ (R)	6.211	0.036	<b>Zr</b> +Rh
$B_{1u}$ (I)	6.416	0.007	<b>Zr</b> +Rh	$B_{1u}$ (I)	9.144	0.018	<b>Si</b>
$B_{1u}$ (I)	9.301	0.017	Rh+ <b>Si</b>	$A_g$ (R)	9.482	0.040	<b>Si</b>
$B_{2g}$ (R)	9.589	0.036	<b>Si</b>	$B_{3u}$ (I)	9.669	0.013	<b>Si</b>
$B_{3u}$ (I)	9.749	0.023	Zr+ <b>Si</b>	$A_g$ (R)	10.459	0.021	<b>Si</b>
$A_u$ (S)	10.483	0.002	<b>Si</b>	$B_{2g}$ (R)	10.510	0.021	Zr+Rh+ <b>Si</b>
$B_{3g}$ (R)	10.569	0.023	<b>Si</b>	$B_{2u}$ (I)	10.813	0.005	<b>Si</b>
$B_{1g}$ (R)	11.239	0.006	<b>Si</b>				



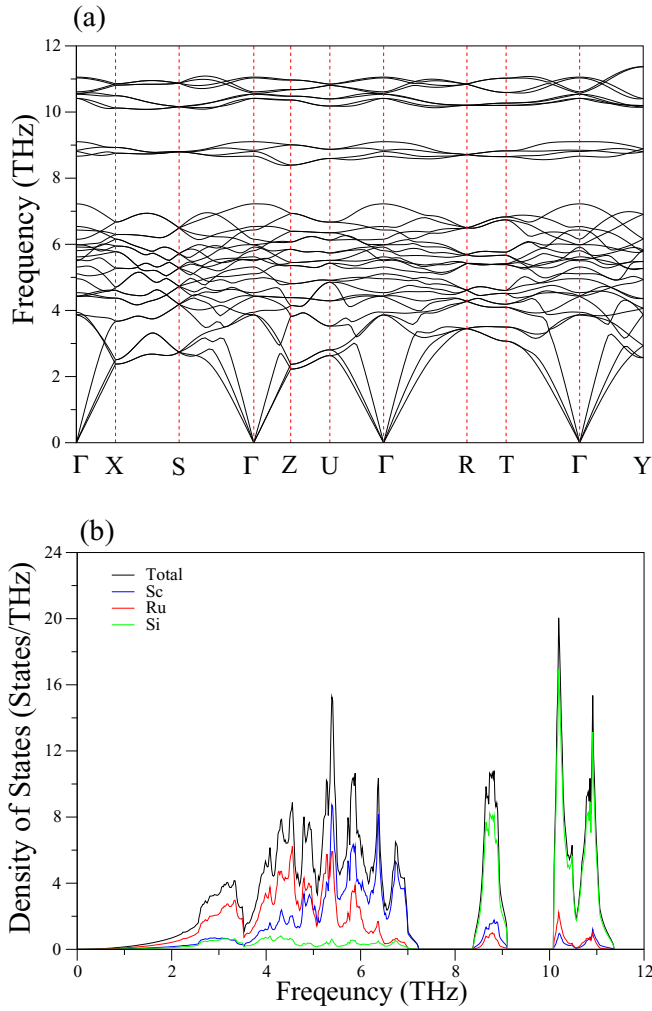


FIG. 6. (a) The calculated phonon spectrum of ScRuSi along the most important axes of symmetry in the Brillouin zone of a simple orthorhombic lattice. (b) Total and partial phonon density of states for ScRuSi.

is observed in the LFB region. Ru, as the heaviest element, dominates the lower frequencies below 4.7 THz. In the entire region from 4.7 to 5.6 THz, a strong Sc-Ru hybridization is present, while the contribution of Sc to the lattice vibrations is the strongest between 5.6 and 7.2 THz.

The phonon band dispersion of ZrRhSi is depicted in Fig. 7(a). Although the electronic structure of ZrRhSi is similar to that of ScRuSi, its phonon structure is different from that of ScRuSi. The phonon spectrum of ZrRhSi is divided into two apparent regions rather than three apparent regions as observed for ScRuSi. The first region extends from 0 to 6.4 THz with 3 acoustic and 21 optical branches, while the high-frequency region lies between 8.9 and 11.6 THz with 12 optical phonon branches. In the low-frequency region, strong coupling exists between low-frequency optical phonon branches and three acoustic phonon branches. The total and partial phonon DOS displayed in Fig. 7(b) suggest that different from ScRuSi, since the masses of Zr and Rh atoms are closer to each other, a strong hybridization between their atomic vibrations exists in the whole low-frequency region

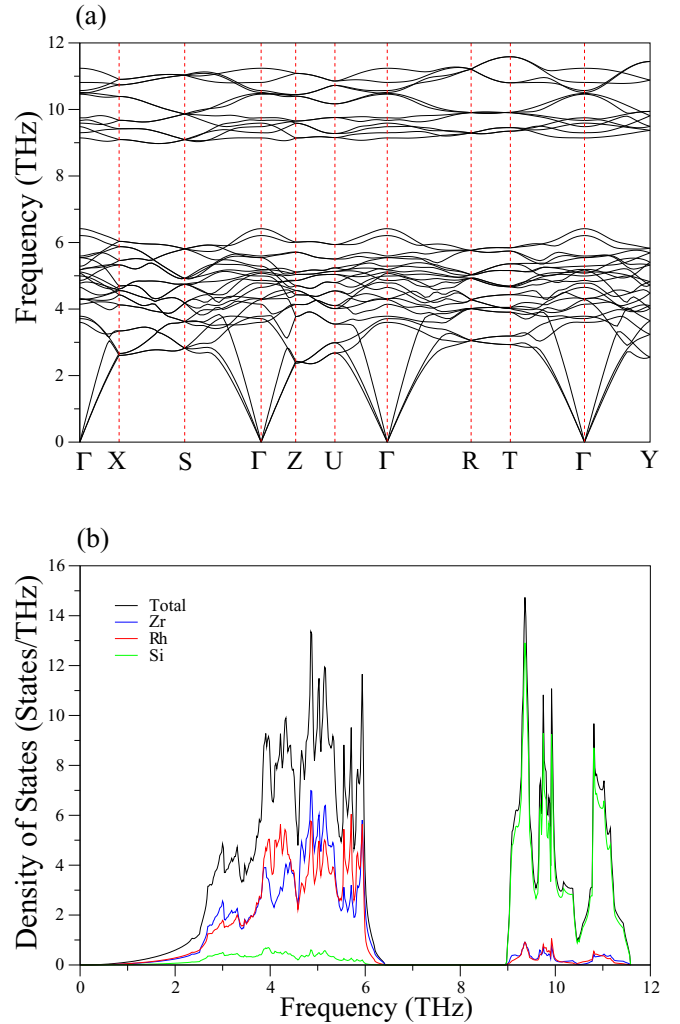


FIG. 7. (a) The calculated phonon spectrum of ZrRhSi along the most important axes of symmetry in the Brillouin zone of a simple orthorhombic lattice. (b) Total and partial phonon density of states for ZrRhSi.

of DOS. In agreement with ScRuSi, the partial DOS shows a dominance of Si atoms in the high-frequency region.

For the orthorhombic system, the acoustic phonon velocities in different directions are connected to elastic constants by the following formulas [73]:

Along the  $\Gamma$ -X ([100]) direction,

$$V_{LA}^{[100]} = \sqrt{C_{11}/\rho}, \quad V_{TA_1}^{[001]} = \sqrt{C_{55}/\rho}, \quad V_{TA_2}^{[010]} = \sqrt{C_{66}/\rho}. \quad (13)$$

Along the  $\Gamma$ -Y ([010]) direction,

$$V_{LA}^{[010]} = \sqrt{C_{22}/\rho}, \quad V_{TA_1}^{[100]} = \sqrt{C_{66}/\rho}, \quad V_{TA_2}^{[001]} = \sqrt{C_{44}/\rho}. \quad (14)$$

Along the  $\Gamma$ -Z ([001]) direction,

$$V_{LA}^{[001]} = \sqrt{C_{33}/\rho}, \quad V_{TA_1}^{[100]} = \sqrt{C_{55}/\rho}, \quad V_{TA_2}^{[010]} = \sqrt{C_{44}/\rho}. \quad (15)$$

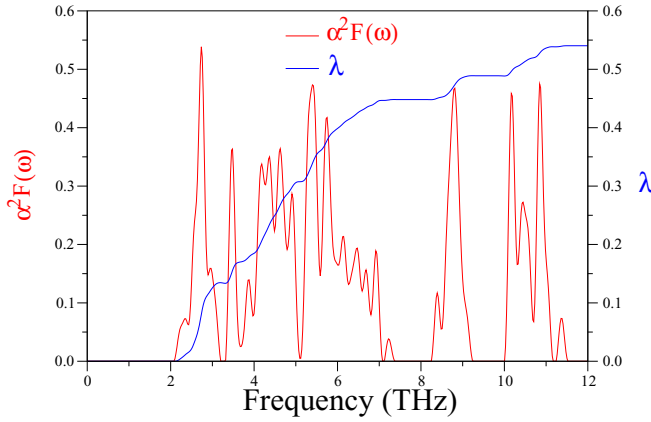


FIG. 8. The Eliashberg spectral function  $\alpha^2 F(\omega)$  (red lines) and the frequency dependence of average electron-phonon coupling parameter  $\lambda$  (blue lines) for ScRuSi.

Having calculated the values of  $V_{TA_1}$ ,  $V_{TA_2}$ , and  $V_{LA}$  from the related phonon spectrum, the related elastic constants are obtained from the above formulas. We have to mention that the average values obtained from the different formulas are utilized for  $C_{44}$ ,  $C_{55}$ , and  $C_{66}$ . Therefore, the values of  $C_{11}$ ,  $C_{22}$ ,  $C_{33}$ ,  $C_{44}$ ,  $C_{55}$ , and  $C_{66}$  for ScRuSi (ZrRhSi) are found to be 236 (284), 257 (256), 191 (290), 62 (115), 61 (110), and 82 (110) GPa. These values are compatible with their corresponding values calculated from the stress-strain method calculations (see also Table II). In particular, the derived value of  $C_{66}$  from the phonon spectrum is almost equal to its value of 85 GPa obtained from the stress-strain method calculations (see also Table II). This agreement supports the accuracy of our GGA calculations.

The Eliashberg spectral function [ $\alpha^2 F(\omega)$ ] and the frequency dependence of the average electron-phonon coupling parameter for ScRuSi are presented in Fig. 8. A comparison of this spectral function with the corresponding phonon DOS shows that the former one is enhanced relative to the latter one in the LFB. This signals that acoustic phonon branches and low-frequency optical phonon branches of ScRuSi couple strongly with electrons at the Fermi level. Consequently, they constitute 84% (0.4536) of  $\lambda$ . This large additive arises from their vibrational patterns since they are mainly characterized by the coupled motion of transition-metal atoms, which dominate energy states in the vicinity of the Fermi level with their  $d$  states. However, Si-related vibrational modes in the MFB and the HFB contribute about 16% (0.0864) to  $\lambda$ . This small additive from Si-related vibrations can be linked to the factor  $\frac{1}{\omega}$  in the integral formula [see also Eq. (4)]. At the end, the total value of  $\lambda$  is calculated to be 0.54 for ScRuSi from the integration of  $\alpha^2 F(\omega)$  [see again Eq. (4)]. This small value reveals that the electron-phonon interaction in ScRuSi is of weak strength.

The Eliashberg spectral function in Fig. 9 for ZrRhSi shows the electron-phonon interaction in this material is much stronger than that in ScRuSi. In agreement with ScRuSi, low-frequency phonon scattering of electrons plays a significant role in the transition from the normal state to the superconducting state for ZrRhSi. In particular, phonon modes in the low-frequency region form 86% (0.7224) of  $\lambda$ , while phonon

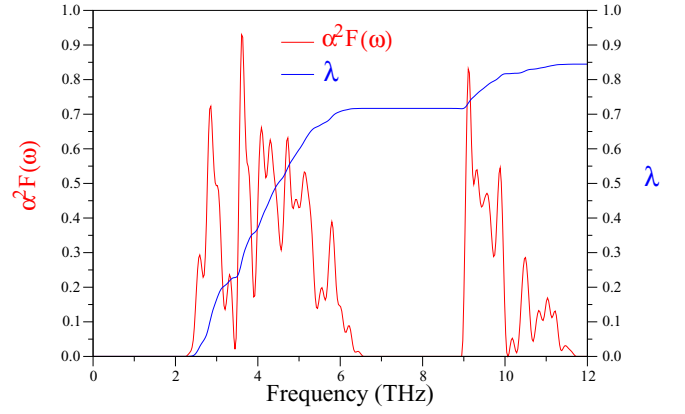


FIG. 9. The Eliashberg spectral function  $\alpha^2 F(\omega)$  (red lines) and the frequency dependence of average electron-phonon coupling parameter  $\lambda$  (blue lines) for ZrRhSi.

modes in the high-frequency region contribute about 14% (0.1176) to  $\lambda$ . The integration of  $\alpha^2 F(\omega)$  [see Eq. (4)] gives the value of  $\lambda$  to be 0.84 for ZrRhSi, which is considerably larger than the corresponding value of 0.54 for ScRuSi. Consequently, ZrRhSi is a phonon-mediated superconductor with intermediate electron-phonon coupling strength rather than with weak electron-phonon coupling strength as observed for ScRuSi.

The Eliashberg spectral function integrates [see Eq. (5)] the logarithmically averaged frequency  $\omega_{\ln}$  value of 227.12 and 213.35 K for ScRuSi and ZrRhSi, respectively. Then, when we insert the calculated values of  $\lambda$  and  $\omega_{\ln}$  into the Allen-Dynes modified McMillan formula [(see Eq. (6)), the value of  $T_c$  is found to be 3.23 K for ScRuSi and 10.45 K for ZrRhSi. These values accord very well with their measured values of 3.1 and 10.3 K [32,42]. Finally, it will be necessary to make a comparison as regards superconductivity between ScRuSi and its isostructural compound ZrRhSi by analyzing their electronic and phonon structures. Before making any discussion, we have to remark that there are three main factors which affect the value of  $T_c$  for BCS-type superconductors. These factors are the electronic DOS at the Fermi level [ $N(E_F)$ ], the logarithmic average phonon frequency ( $\omega_{\ln}$ ), and the strength of the electron-phonon coupling parameter ( $\lambda$ ). As regards the electronic structure, the value of  $N(E_F)$  decreases from 9.848 to 8.474 states/eV when our material is changed from ScRuSi to ZrRhSi. This change influences the value of  $\lambda$  because  $\lambda$  is directly connected to the change in  $N(E_F)$  due to the McMillan-Hopfield expression ( $\lambda = \frac{N(E_F)\langle I^2 \rangle}{M\langle \omega^2 \rangle}$ ) [60], where  $N(E_F)$  represents the density of states at the Fermi level,  $\langle I^2 \rangle$  gives the averaged square of the electron-phonon matrix element,  $\langle \omega^2 \rangle$  depicts the averaged square of the phonon frequency, and  $M$  refers to the mass involved. Although harder phonon frequencies give rise to larger  $\omega_{\ln}$  values for ScRuSi, they reduce the value of  $\lambda$  according to the McMillan-Hopfield expression. In this way, the  $\lambda$  value of 0.54 for ScRuSi becomes smaller than the value of 0.84 for ZrRhSi. Eventually, the  $T_c$  value of 3.23 K for ScRuSi becomes significantly lower than the corresponding value of 10.45 K for ZrRhSi.

#### IV. SUMMARY

In this theoretical study, we have aimed to discuss the characteristic features of the superconductivity in the newly discovered superconductor ScRuSi via comparison with its isostructural compound of ZrRhSi by investigating their structural, electronic, elastic, mechanical, phononic, and electron-phonon interaction properties in detail. The calculated lattice parameters of both studied compounds agree very well with their measured values. The calculated elastic constants of both studied compounds meet the stability criteria of an orthorhombic lattice, indicating their mechanical stability in the orthorhombic TiNiSi-type layer structure. An examination of their Cauchy pressures signals stronger metallic bonding in ScRuSi as compared to ZrRhSi. Our results indicate that ScRuSi is ductile, while its isostructural ZrRhSi is a brittle compound.

The energy bands in the vicinity of the Fermi level arise from the  $d$  states of transition-metal atoms. Although their electronic structures are similar to each other, their phonon structures are different from each other. For both compounds, low-frequency phonon modes constitute more than 80% of the average electron-phonon coupling parameter. This

large contribution has been related with the origin of these phonon modes because they arise from the coupled motion of transition-metal atoms, which dominate energy bands in the vicinity of the Fermi level with their  $d$  states.

Finally, the calculations give the value of 0.54 for ScRuSi which is smaller than the value of 0.84 for ZrRhSi. The value of the average electron-phonon coupling parameter is found to be 0.54 for ScRuSi and 0.84 for ZrRhSi. These results indicate that while both compounds are phonon-mediated superconductors, the weaker electron-phonon interaction in ScRuSi makes the superconducting transition temperature of ScRuSi considerably lower than that of ZrRhSi. The superconducting transition temperature is estimated to be 3.23 K for ScRuSi and 10.45 K for ZrRhSi, which are in excellent coherence with their experimental values of 3.1 and 10.3 K, respectively. Finally, we strongly believe that this study can provide theoretical guidance for future investigations on the ternary equiatomic intermetallic compounds.

#### ACKNOWLEDGMENT

Numerical calculations were performed using the Intel Nehalem (i7) cluster (ceres) at the University of Exeter.

- 
- [1] C. B. Shoemaker and D. P. Shoemaker, A ternary alloy with PbCl<sub>2</sub>-type structure: TiNiSi( $E$ ), *Acta Cryst.* **18**, 900 (1965).
- [2] A. E. Dwight, M. H. Mueller, R. A. Conner, Jr., J. W. Downey, and H. Knott, Ternary compounds with the Fe<sub>2</sub>P-type structure, *Trans. Metall. Soc. AIME* **242**, 2075 (1968).
- [3] N. Chaichit, P. Chalugune, S. Rukvichai, P. Choosang, V. Kaewchansilp, C.-O. Pontchour, P. Phavanantha, and S. Pramatus, Crystal structure refinements of ZrCoP, NbCoP, NbNiP and TaFeP, *Acta Chem. Scand. A* **32**, 309 (1978).
- [4] W. Jeitschko and E. J. Reinbold, Structural chemistry of new scandium cobalt phosphides with a metal: Phosphorus ratio of 2:1, *Z. Naturforsch. B* **40**, 900 (1985).
- [5] Ya. F. Lomnytska and Yu. B. Kuz'ma, New phosphides of IVa and Va group metals with TiNiSi-type, *J. Alloys Compd.* **269**, 133 (1998).
- [6] M. F. Zumdick, R. D. Hoffmann, and R. Pöttgen, The intermetallic zirconium compounds ZrNiAl, ZrRhSn, and ZrPtGa—structural distortions and metal-metal bonding in Fe<sub>2</sub>P related compounds, *Z. Naturforsch. B* **54**, 45 (1999).
- [7] U. Pfannenschmidt, U. Ch. Rodewald, and R. Pöttgen, ScIrP with ZrNiAl-type structure, *Z. Naturforsch. B* **66**, 205 (2011).
- [8] T. Dinges, M. Eul, and R. Pöttgen, TaRhGe with TiNiSi-type structure, *Z. Naturforsch. B* **65**, 95 (2010).
- [9] R.-D. Hoffmann, U. Ch. Rodewald, S. Haverkamp, C. Benndorf, H. Eckert, B. Heying, and R. Pöttgen, The high-temperature modification of ScRuSi—Structure, <sup>29</sup>Si and <sup>45</sup>Sc solid state NMR spectroscopy, *Solid State Sci.* **72**, 109 (2017).
- [10] S. Stein, T. Block, S. Klenner, L. Heletta, and R. Pöttgen, Equiatomic iron-based tetrelides TFeSi and TFeGe ( $T = \text{Zr, Nb, Hf, Ta}$ )—A <sup>57</sup>Fe Mössbauer-spectroscopic study, *Z. Naturforsch. B* **74**, 211 (2019).
- [11] T. Eriksson, L. Bergqvist, T. Burkert, S. Felton, R. Tellgren, P. Nordblad, O. Eriksson, and Y. Andersson, Cycloidal magnetic order in the compound IrMnSi, *Phys. Rev. B* **71**, 174420 (2005).
- [12] G. J. Li, E. K. Liu, H. G. Zhang, Y. J. Zhang, J. L. Chen, W. H. Wang, H. W. Zhang, G. H. Wu, and S. Y. Yu, Phase diagram, ferromagnetic martensitic transformation and magnetoresponse properties of Fe-doped MnCoGe alloys, *J. Magn. Magn. Mater.* **332**, 146 (2013).
- [13] Z. Wang, Z. Nie, J. Zeng, R. Su, Y. Zhang, D. E. Brown, Y. Ren, and Y. Wang, First-order magnetostructural transformation in Fe doped Mn-Co-Ge alloys, *J. Alloys Compd.* **577**, 486 (2013).
- [14] J. Zeng, Z. Wang, Z. Nie, and Y. Wang, Crystal structural transformation accompanied by magnetic transition in MnCo<sub>1-x</sub>Fe<sub>x</sub>Ge alloys, *Intermetallics* **52**, 101 (2014).
- [15] P. Dutta, S. Pramanick, S. Majumdar, D. Das, and S. Chatterjee, Multifunctional behavior of Fe-doped MnNiGe magnetic equiatomic compound, *J. Magn. Magn. Mater.* **395**, 312 (2015).
- [16] S. C. Ma, Y. Su, M. Yang, F. Yang, Y. L. Huang, K. Liu, L. Zhang, and Z. C. Zhong, Magnetic phase transition and magnetocaloric effect in Mn-Fe-Ni-Ge ribbons, *J. Alloys Compd.* **629**, 322 (2015).
- [17] J. Liu, Y. Si, Y. Gong, G. Xu, E. Liu, F. Xu, and D. Wang, Enhanced magnetic refrigeration performance in metamagnetic MnCoSi alloy by high-pressure annealing, *J. Alloys Compd.* **701**, 858 (2017).
- [18] S. C. Ma, Q. Ge, S. Yang, K. Yu, X. Q. Han, K. Liu, Y. Song, L. L. Zhang, Q. Z. Jiang, M. L. Zhong, R. H. Liu, L. Wang, J. J. Li, and Z. C. Zhong, Investigation of the martensitic microstructure and magnetostructural coupling in rapidly solidified Mn-Ni-Fe-Ge rod samples, *J. Alloys Compd.* **729**, 1190 (2017).
- [19] M. Onoue, R. Kobayashi, Y. Mitsui, M. Hiroi, K. Takahashi, A. Kondo, K. Kindo, Y. Uwatoko, and K. Koyama, Magnetic and structural properties of MnCoGe with minimal Fe and Sn substitution, *Mater. Trans.* **59**, 1645 (2018).
- [20] J. Q. Zhao, H. X. Zhu, C. L. Zhang, Y. G. Nie, H. F. Shi, E. J. Ye, Z. D. Han, and D. H. Wang, Magnetostructural transition

- and magnetocaloric effect in a MnCoSi-based material system, *J. Alloys Compd.* **735**, 959 (2018).
- [21] C. L. Zhang, Y. G. Nie, H. F. Shi, E. J. Ye, Z. D. Han, and D. H. Wang, Tuning magnetostructural transition and the associated giant magnetocaloric effect via thermal treatment in MnCoGe-based alloys, *J. Magn. Magn. Mater.* **469**, 437 (2019).
- [22] H. Barz, H. C. Ku, G. P. Meisner, Z. Fisk, and B. T. Matthias, Ternary transition metal phosphides: High-temperature superconductors, *Proc. Natl. Acad. Sci. USA* **77**, 3132 (1980).
- [23] G. P. Meisner and H. C. Ku, The superconductivity and structure of equiatomic ternary transition metal pnictides, *Appl. Phys. A* **31**, 201 (1983).
- [24] G. P. Meisner, H. C. Ku, and H. Barz, Superconducting equiatomic ternary transition metal arsenides, *Mater. Res. Bull.* **18**, 983 (1983).
- [25] R. Muller, R. N. Shelton, J. W. Richardson, Jr., and R. A. Jacobson, Superconductivity and crystal structure of a new class of ternary transition metal phosphides  $TT'P$  ( $T = \text{Zr, Nb, Ta}$  and  $T' = \text{Ru, Rh}$ ), *J. Less-Common Met.* **92**, 177 (1983).
- [26] H. Keiber, H. Wuhl, G. P. Meisner, and G. R. Stewart, Phonon anomalies in ZrRuP, *Low Temp. Phys.* **55**, 11 (1984).
- [27] W. Xian-Zhong, B. Chevalier, J. Etourneau, and P. Hagenmuller, New superconducting equiatomic ternary silicides  $M\text{IrSi}$  ( $M = \text{Y, Zr, Hf}$ ) with  $\text{TiNiSi}$ -type structure (anti- $\text{PbCl}_2$ ), *Mater. Res. Bull.* **20**, 517 (1985).
- [28] I. Shirovani, N. Ichihashi, K. Nozawa, M. Kinoshita, T. Yagi, K. Suzuki, and T. Enoki, Superconductivity of ZrRuP, *Jpn. J. Appl. Phys.* **32**, 695 (1993).
- [29] I. Shirovani, K. Tachi, N. Ichihashi, T. Adachi, T. Kikegawa, and O. Shimomura, Phase-transition of ZrRuP at high-temperatures and high-pressures, *Phys. Lett. A* **205**, 77 (1995).
- [30] I. Shirovani, K. Tachi, K. Takeda, S. Todo, T. Yagi, and K. Kanoda, Superconductivity of ZrRuSi prepared at high-pressure, *Phys. Rev. B* **52**, 6197 (1995).
- [31] H. Salamati, F. S. Razavi, and G. Quirion, Effect of pressure on the superconductivity of ZrRuP, *Physica C* **292**, 79 (1997).
- [32] I. Shirovani, Y. Konno, Y. Okada, C. Sekine, S. Todo, and T. Yagi, Superconductivity of  $\text{MRhSi}$  ( $M = \text{Ti, Zr}$  and  $\text{Hf}$ ), *Solid State Commun.* **108**, 967 (1998).
- [33] I. Shirovani, M. Takaya, I. Kaneko, C. Sekine, and T. Yagi, Superconductivity of  $\text{MRuP}$  and  $\text{MNiP}$  ( $M = \text{Mo}$  or  $\text{W}$ ) prepared at high pressure, *Solid State Commun.* **116**, 683 (2000).
- [34] D. C. Kundaliya and S. K. Malik, Superconductivity in the intermetallic compound  $\text{YRhAl}$ , *Solid State Commun.* **131**, 489 (2004).
- [35] K. Kudo, K. Fujimura, S. Onari, H. Ota, and M. Nohara, Superconductivity in  $\text{MgPtSi}$ : An orthorhombic variant of  $\text{MgB}_2$ , *Phys. Rev. B* **91**, 174514 (2015).
- [36] T. Harmening, H. Eckert, C. M. Fehse, C. P. Sebastian, and R. Pöttgen, Sc-45 solid state NMR studies of the silicides  $\text{ScTSi}$  ( $T = \text{Co, Ni, Cu, Ru, Rh, Pd, Ir, Pt}$ ), *J. Solid State Chem.* **184**, 3303 (2011).
- [37] B. Heying, S. Haverkamp, Ute Ch Rodewald, H. Eckert, S. C. Peter, and R. Pöttgen, The germanides  $\text{ScTGe}$  ( $T = \text{Co, Ni, Cu, Ru, Rh, Pd, Ag, Ir, Pt, Au}$ )-Structure and  $^{45}\text{Sc}$  solid state NMR spectroscopy, *Solid State Sci.* **39**, 15 (2015).
- [38] J. J. Hamlin and J. S. Schilling, Pressure-induced superconductivity in Sc to 74 GPa, *Phys. Rev. B* **76**, 012505 (2007).
- [39] M. Debessai, J. J. Hamlin, and J. S. Schilling, Comparison of the pressure dependences of  $T_c$  in the trivalent  $d$ -electron superconductors Sc, Y, La, and Lu up to megabar pressures, *Phys. Rev. B* **78**, 064519 (2008).
- [40] Y. Okamoto, T. Inohara, Y. Yamakawa, A. Yamakage, and K. Takenaka, Superconductivity in the hexagonal ternary phosphide  $\text{ScIrP}$ , *J. Phys. Soc. Jpn.* **85**, 013704 (2016).
- [41] T. Inohara, Y. Okamoto, Y. Yamakaw, and K. Takenaka, Synthesis and superconducting properties of a hexagonal phosphide  $\text{ScRhP}$ , *J. Phys. Soc. Jpn.* **85**, 094706 (2016).
- [42] B.-B. Ruan, X.-C. Wang, J. Yu, B.-J. Pan, Q.-G. Mu, T. Liu, G.-F. Chen, and Z.-A. Ren, Superconductivity at 3.1 K in the orthorhombic ternary silicide  $\text{ScRuSi}$ , *Supercond. Sci. Technol.* **30**, 025008 (2017).
- [43] D. K. Seo, J. Ren, M. H. Whangbo, and E. Canadell, Electronic band structure study of the transport properties of the intermetallic compounds  $\text{ZrRuP}$  and  $\text{ZrRuSi}$ , *Inorg. Chem.* **36**, 6058 (1997).
- [44] I. Hase, Electronic structure of superconducting compounds  $\text{h-ZrRuX}$  ( $X = \text{P, As, Si}$ ), *Phys. Rev. B* **65**, 174507 (2002).
- [45] W. Y. Ching, Y.-N. Xu, L. Ouyang, and W. Wong-Ng, Comparative study of the electronic structure of ternary superconductors  $\text{MoRuP}$  and  $\text{ZrRuP}$  in the orthorhombic and hexagonal phases, *J. Appl. Phys.* **93**, 8209 (2003).
- [46] N. Sebehi, Kh. Bouamama, Ph. Djemia, and K. Kassali, Structural and elastic properties of ternary silicides  $\text{ScTSi}$  ( $T = \text{Co, Ni, Cu, Ru, Rh, Pd, Ir, Pt}$ ) and of the equiatomic intermetallic compounds  $\text{YTX}$  ( $T = \text{Ni, Ir}$  and  $X = \text{Si, Ge, Sn, Pb}$ ), *Phys. Status Solidi B* **252**, 2769 (2015).
- [47] H. M. Tütüncü, E. Karaca, and G. P. Srivastava, Ab initio investigation of superconductivity in orthorhombic  $\text{MgPtSi}$ , *J. Alloys Compd.* **673**, 302 (2016).
- [48] A. S. Cuamba, H.-Y. Lu, and C. S. Ting, Electronic structure and phonon-mediated superconductivity in  $\text{ScIrP}$  compound: First-principles calculations, *Phys. Rev. B* **94**, 094513 (2016).
- [49] S. Bağcı, M. Cin, H. Y. Uzunok, E. Karaca, H. M. Tütüncü, and G. P. Srivastava, Investigating the normal state and superconducting state properties of orthorhombic and hexagonal  $\text{ZrRuP}$ : A first-principles study, *Phys. Rev. B* **100**, 184507 (2019).
- [50] A. Dal Corso, Elastic constants of beryllium: A first-principles investigation, *J. Phys.: Condens. Matter* **28**, 075401 (2016).
- [51] A. B. Migdal, Interaction between electrons and lattice vibrations in a normal metal, *Zh. Eksp. Teor. Fiz.* **34**, 996 (1958).
- [52] G. M. Eliashberg, Interaction between electrons and lattice vibrations in a superconductor, *Sov. Phys. JETP* **11**, 696 (1960).
- [53] P. Giannozzi, S. Baroni, N. Bonini, M. Calandra, R. Car, C. Cavazzoni, D. Ceresoli, G. L. Chiarotti, M. Cococcioni, I. Dabo, A. Dal Corso, S. de Gironcoli, S. Fabris, G. Fratesi, R. Gebauer, U. Gerstmann, C. Gougoussis, A. Kokalj, M. Lazzeri, L. Martin-Samos, N. Marzari, F. Mauri, R. Mazzarello, S. Paolini, A. Pasquarello, L. Paulatto, C. Sbraccia, S. Scandolo, G. Sclauzero, A. P. Seitsonen, A. Smogunov, P. Umari, and R. M. Wentzcovitch, QUANTUM ESPRESSO: A modular and open-source software project for quantum simulations of materials, *J. Phys.: Condens. Matter* **21**, 395502 (2009).
- [54] P. Giannozzi, O. Andreussi, T. Brumme, O. Bunau, M. Buongiorno Nardelli, M. Calandra, R. Car, C. Cavazzoni, D. Ceresoli, M. Cococcioni, N. Colonna, I. Carnimeo, A. Dal Corso, S. de Gironcoli, P. Delugas, R. A. DiStasio, Jr., A. Ferretti, A. Floris, G. Fratesi, G. Fugallo, R. Gebauer, U. Gerstmann, F. Giustino, T. Gorni, J. Jia, M. Kawamura, H.-Y. Ko, A. Kokalj, E. Küçükbenli, M. Lazzeri, M. Marsili,

- N. Marzari, F. Mauri, N. L. Nguyen, H.-V. Nguyen, A. Otero-de-la-Roza, L. Paulatto, S. Ponc e, D. Rocca, R. Sabatini, B. Santra, M. Schlipf, A. P. Seitsonen, A. Smogunov, I. Timrov, T. Thonhauser, P. Umari, N. Vast, X. Wu, and S. Baroni, Advanced capabilities for materials modelling with Quantum ESPRESSO, *J. Phys.: Condens. Matter* **29**, 465901 (2017).
- [55] J. P. Perdew, K. Burke, and M. Ernzerhof, Generalized Gradient Approximation Made Simple, *Phys. Rev. Lett.* **77**, 3865 (1996).
- [56] R. Stumpf, X. Gonze, and M. Scheffler, A list of separable, norm-conserving, *ab initio* pseudopotentials, Fritz-Haber-Institut report, Berlin, 1990.
- [57] T. H. Fischer and J. Almlof, General methods for geometry and wave function optimization, *J. Phys. Chem.* **96**, 9768 (1992).
- [58] W. Kohn and L. J. Sham, Self-consistent equations including exchange and correlation effects, *Phys. Rev.* **140**, A1133 (1965).
- [59] H. J. Monkhorst and J. D. Pack, Special points for Brillouin-zone integrations, *Phys. Rev. B* **13**, 5188 (1976).
- [60] W. L. McMillan, Transition temperature of strong-coupled superconductors, *Phys. Rev.* **167**, 331 (1968).
- [61] P. B. Allen and R. C. Dynes, Transition temperature of strong-coupled superconductors reanalyzed, *Phys. Rev. B* **12**, 905 (1975).
- [62] P. B. Allen and R. C. Dynes, Superconductivity at very strong coupling, *J. Phys. C: Solid State Phys.* **8**, L158 (1975).
- [63] H. M. T utt nc u, H. Y. Uzunok, E. Karaca, G. P. Srivastava, S.  zer, and  . U ur, *Ab initio* investigation of BCS-type superconductivity in LuNi<sub>2</sub>B<sub>2</sub>C-type superconductors, *Phys. Rev. B* **92**, 054510 (2015).
- [64] A. Kokalj, XCRYSDEN—a new program for displaying crystalline structures and electron densities, *J. Mol. Graphics Modell.* **17**, 176 (1999).
- [65] Z.-J. Wu, E.-J. Zhao, H.-P. Xiang, X.-F. Hao, X.-J. Liu, and J. Meng, Crystal structures and elastic properties of superhard IrN<sub>2</sub> and IrN<sub>3</sub> from first principles, *Phys. Rev. B* **76**, 054115 (2007).
- [66] D. Farkas, Interatomic potentials for Ti-Al with and without angular forces, *Modell. Simul. Mater. Sci. Eng.* **2**, 975 (1994).
- [67] W. Voigt, *Lehrbuch der Kristallphysik* (Teubner, Leipzig, 1928).
- [68] A. Reuss, Berechnung der Fliegrenze von Mischkristallen auf Grund der Plastizit tsbedingung f r Einkristalle, *Z. Angew. Math. Mech.* **9**, 49 (1929).
- [69] R. Hill, The elastic behaviour of a crystalline aggregate, *Proc. Phys. Soc. Sect. A* **65**, 349 (1952).
- [70] S. F. Pugh, XCII. Relations between the elastic moduli and the plastic properties of polycrystalline pure metals, *Philos. Mag.* **45**, 823 (1954).
- [71] J. Haines, J. M. Leger, and G. Bocquillon, Synthesis and design of superhard materials, *Annu. Rev. Mater. Res.* **31**, 1 (2001).
- [72] P. Ravindran, L. Fast, P. A. Korzhavyi, B. Johansson, J. Wills, and O. Eriksson, Density functional theory for calculation of elastic properties of orthorhombic crystals: Application to TiSi<sub>2</sub> *J. Appl. Phys.* **84**, 4891 (1998).
- [73] L. J. Liu, L. Lian, and J. Yu, Stability, mechanical properties and anisotropic elastic properties of Ga<sub>3</sub>Mg<sub>3</sub> compounds, *Mater. Res.* **22**, e201800624 (2019).